BONTHRON EDITED

ORIGINAL ARTICLE

Cousins not twins: intra and inter-tumoral heterogeneity in syndromic neuroendocrine tumours

Aidan Flynn[1,2], Trisha Dwight[3,4], Diana Benn[3,4], Siddhartha Deb[5], Andrew J Colebatch[1,2], Stephen Fox[1,2,6], Jessica Harris[7], Emma L Duncan[7,8,9], Bruce Robinson[3,4] Annette Hogg[1], Jason Ellul[1], Henry To[10], Cuong Duong[1], Julie A Miller[10, 11], Christopher Yates[12,13], Paul James[1,6], Alison Trainer[1,2], Anthony J Gill[4,14], Roderick Clifton-Bligh[3,4], Rodney J Hicks[1,6], Richard W Tothill[1,2,6, *]

1. The Peter MacCallum Cancer Centre, East Melbourne, VIC, Australia
2. The Department of Pathology, University of Melbourne, Parkville, VIC, Australia
3. Cancer Genetics, Kolling Institute, Royal North Shore Hospital, Sydney, NSW, Australia
4. University of Sydney, Sydney, NSW, Australia
5. Anatomical Pathology, Anatpath, Gardenvale, VIC, Australia
6. The Sir Peter MacCallum Department of Oncology, The University of Melbourne, Parkville, VIC, Australia.
7. Queensland University of Technology, Brisbane, Australia
8 Faculty of Medicine, University of Queensland, Brisbane, Australia
9. Department of Endocrinology, Royal Brisbane and Women's Hospital, Brisbane
10. Department of Surgery, Royal Melbourne Hospital, Parkville, VIC, Australia
11. Department of Surgery, Epworth Hospital, Richmond, VIC, Australia
12. Department of Diabetes and Endocrinology, Royal Melbourne Hospital, VIC, Australia
13. Department of Diabetes and Endocrinology, Western Health, VIC, Australia
14. The Department of Anatomical Pathology, Royal North Shore Hospital, Sydney, NSW, Australia

* Corresponding author.

richard.tothill@petermac.org

Phone: +61 3 9656 1752

FAX: +61 3 9656 1414

Running title: Heterogeneity in familial neuroendocrine tumours

Conflict of interest statement: The authors have no conflicts of interest to disclose

Word count: 4000

Data Availability

This is the author manuscript accepted for publication and has undergone full peer review but has not been through the copyediting, typesetting, pagination and proofreading process, which may lead to differences between this version and the Version of Record. Please cite this article as doi: 10.1002/path.4900

This article is protected by copyright. All rights reserved.

Author Manuscript

Affymetrix Cytoscan HD and Oncoscan array data are available through NCBI GEO (http://www.ncbi.nlm.nih.gov/geo/, GEO Accession: GSE94378

Author Manuscript

This article is protected by copyright. All rights reserved.

Abstract

Hereditary endocrine neoplasias, including phaeochromocytoma/paraganglioma and medullary thyroid cancer, are caused by autosomal dominant mutations in several familial cancer genes. A common feature of these diseases is the presentation of multiple primary tumours, or multifocal disease representing independent tumour clones that have arisen from the same initiating genetic lesion, but have undergone independent clonal evolution. Such tumours provide an opportunity to discover common co-operative changes required for tumorigenesis, while controlling for the genetic background of the individual. We performed genomic analysis of synchronous and metachronous tumours from five patients bearing germline mutations in the genes *SDHB*, *RET* and *MAX*. Using whole exome sequencing and high-density SNP arrays, we analyzed two to four primary tumours from each patient. We also applied multi-regional sampling, to assess intra-tumoral heterogeneity and clonal evolution, in two cases involving phaeochromocytoma/paraganglioma and medullary thyroid cancer, respectively. Heterogeneous patterns of genomic change existed between synchronous or metachronous tumours, with evidence of branching evolution. We observed striking examples of evolutionary convergence involving the same rare somatic copy-number events in synchronous primary phaeochromocytoma/paraganglioma. Convergent events also occurred during clonal evolution of metastatic medullary thyroid cancer. These observations suggest that genetic or epigenetic changes acquired early within precursor cells, or pre-existing within the genetic background of the individual, create contingencies that determine the evolutionary trajectory of the tumour.

Key Words

This article is protected by copyright. All rights reserved.

Author Manuscript

tumour heterogeneity, neoplasia, pheochromocytoma, paraganglioma, medullary thyroid cancer, genomics, hereditary endocrine neoplasia

Author Manuscript

This article is protected by copyright. All rights reserved.

Introduction

Endocrine tumours arise from tissues of the pituitary, thyroid, parathyroid, pancreas, adrenal and sympathetic paraganglia. Although rare, these tumours have a high burden of disease owing to metastatic disease in some individuals, compression effects of tumour growth and excess hormone secretion. A significant fraction of cases arise in the context of heritable tumour syndromes[1]. For example, multiple endocrine neoplasia type 2 (MEN2) is caused by mutations in the proto-oncogene *RET* and can involve both medullary thyroid carcinoma (MTC) and phaeochromocytoma. Phaeochromocytomas and extra-adrenal paragangliomas (collectively termed PPGL) are also caused by germline mutations in other genes (e.g. *VHL*, *NF1*, *SDHA-D*, *TMEM127*, *MAX*)[2]. Although these genes are ostensibly the principal drivers of disease, additional somatic events are required for tumorigenesis. Identifying these secondary and tertiary genetic lesions and the timing of these events is important to better understand disease biology, the potential cause of different clinical behaviours between individuals and to identify new therapeutic vulnerabilities.

The clonal evolution of cancer can be inferred from multi-regional or temporal sampling of tumour tissues in individual patients. This approach has been adopted in multiple tumour types including colon[3], prostate[4,5], lung[6,7], kidney[8], ovary[9], and brain[10]. These explorations of tumour heterogeneity provide insight into the selective pressures acting on a developing tumour, as well as demonstrating examples of evolutionary convergence that highlight co-operative oncogenic events[11]. Genomic profiling of familial cancers provides an additional view of tumour evolution, by enabling analysis of parallel evolution in multiple primaries or multifocal disease [8]. In PPGL, somatic copy-number profiling and whole

This article is protected by copyright. All rights reserved.

Author Manuscript

exome sequencing (WES) have been used in a small number of cases to examine tumour evolution through the lens of intra-tumoral heterogeneity[12-14]. However, how evolutionary concepts such as contingency and convergence contribute to the development of multifocal PPGL or MTC has yet to be explored. In this study, we have therefore searched for common genetic changes in synchronous and metachronous PPGL and MTC in addition to mapping the clonal evolution of these tumours by multi-region analysis.

Methods

Sample collection

Patient consent and Institutional Review Board approval were obtained according to the guidelines of the Australian National Health and Medical Research Council in accordance with the Helsinki Declaration of 1975, as revised in 1983. Biospecimens were collected from the Peter MacCallum Cancer Centre (Protocol: 10/119, accepted 18th Jan 2011), the Victorian Cancer Biobank (Protocol: 2001.116, accepted 15th Aug 2001 and Protocol 98/36, accepted 16th Aug 1998), and the Kolling Institute Neuroendocrine Tumour Bank (Protocol: 0211-171M, accepted 24th March 2003). Patient clinical information, genotype and samples analysed are summarised in Table 1.

Whole exome sequencing

Cellular DNA and circulating cell free DNA (cfDNA) was extracted from tissue, plasma or whole blood samples by column chromatography (Qiagen, Germany). WES of tissue and blood samples was done using Agilent SureSelect V5 (Agilent, CA, USA) or Nimblegen Human Exome V2 (Roche Nimblegen, WI, USA) target enrichment according to the

This article is protected by copyright. All rights reserved.

Author Manuscript

manufacturers' protocols. For WES of cfDNA, libraries were prepared using ThruPLEX-FD library preparation kit (Rubicon Genomics, MI, USA) and captured using Nimblegen Human Exome V2 kit. WES libraries were sequenced on either Illumina HiSeq2500 or Next-Seq platforms (Illumina, CA, USA). Read alignment, variant calling and *post hoc* filtering of data was done as previously described[14]. Briefly, sequencing reads were aligned to the hg19 reference genome using BWA-mem[15]. Single nucleotide variants, small insertions and deletions were detected using muTect[16], JointSNVMix[17], SomaticSniper[18], VarScan[19], and the GATK UnifiedGenotyper and IndelGenotyper[20]. High-confidence variants had an allele frequency >10%, were called by muTect or at least two other callers, and were supported by bidirectional reads.

Variant validation

PCR primers that amplify across variant base positions contained universal 5-prime sequence to be compatible with Fluidigm CS1 and CS2 primers (Fluidigm, CA, USA). Following PCR amplification of genomic DNA, PCR products were pooled and then subjected to secondary PCR using indexed Fluidigm CS1 and CS2 primers (Fluidigm, CA, USA) to create Illumina-compatible libraries before sequencing on MiSeq (2 × 150bp) (Illumina, CA, USA). Read alignment and variant calling were done as previously described[21].

Somatic copy-number analysis

SNP array analysis was performed for fresh and FFPE tissue samples using Affymetrix Cytoscan HD arrays and Oncoscan FFPE Assay Kit (Affymetrix, CA, USA), respectively, according to the manufacturer's protocol. Analysis of SNP array data was done as previously

This article is protected by copyright. All rights reserved.

Author Manuscript

described[14]. Allele-specific copy number was determined from WES data using the tool Sequenza[22].

Analysis of sub-clonal architecture

The PyClone software tool (Version 0.12.3) was used to infer clonal population structure within tumours subjected to multi-region sampling[23]. Variant allele frequencies (VAF) of high-confidence variants occurring in one or more regions of the tumour were supplied to the algorithm. The software was operated with variant priors determined by total copy-number.

Compilation of somatic copy-number frequency from published datasets

Gene expression and SNP array copy-number data were obtained for previously published datasets[13,14]. Specimens with matching gene expression and copy-number data were classified into four PPGL subtypes using a support vector machine, as previously described[24]. Segmentation of SNP array data was performed using the CopyNumber package for R. For the purpose of identifying large segmental changes, segments separated by less than 20 kb sharing the same copy state were joined and segments containing <1000 probes excluded. Specimens were stratified by biological subtype and the chromosomal alteration frequency in each population was calculated for 200-kb windows along each chromosome. The alteration frequency for each chromosomal arm was taken as the median value of all windows. The probability of observing common SCNA events in at least two primary tumours was calculated assuming binomial distribution:

Let X= number of tumours observed with SCNA feature

Let ² = loss occurs on the same copy

This article is protected by copyright. All rights reserved.

Probability of observing exactly x tumours with SCNA feature involving the same chromosome copy is

P(X=x and ²) = P(X=x) P(² | X=x)

= P(X=x) P(²) as the events are independent

$=\binom{n}{x} p^x(1-p)^{n-x}0.5^{x-1}$ where n=number of tumours sampled, p is the probability of observing the SCNA event and 0.5 is the probability of the SCNA event involving the same chromosome copy.

P(Xex and ²) = P(X=x and ²) + P(X=x+1 and ²) + … + P(X=n and ²)

Author Manuscript

This article is protected by copyright. All rights reserved.

Results

Multi-primary and multi-region analysis of SDHB-paraganglioma

We performed an in-depth analysis of an index case (C1) representing a 23-year old male presenting with synchronous primary abdominal paragangliomas (PGL). PET/CT imaging with ^{18}F-FDG identified four retroperitoneal masses: a soft tissue mass located immediately above the left renal vein contiguous with the left adrenal gland and anterior to the left renal hilum (PGL1), a left para-aortic mass at L2 (PGL2), and aortocaval masses at the levels of L2 (PGL3) and L3/4 (PGL4) (**Figure 1A**). Additional staging with ^{68}Ga-DOTA-octreotate (GaTate) showed uptake in PGL3 and PGL4, whereas PGL1 demonstrated heterogeneous uptake suggestive of necrotic regions, and PGL2 had only minimal avidity (**Figure 1A**). The patient underwent laparotomy with en bloc resection of all four tumours. Histopathological review revealed four encapsulated paragangliomas of similar histology. Genetic testing revealed a single base frameshift deletion resulting in a premature stop codon in *SDHB* (NM_003000: c.88delG, NP_002991: p.Gln30ArgfsTer47).

Fresh tissue sections of tumours PGL1 to PGL4 were excised for genomic analysis (**Figure 1B**). A single representative piece from each tumour was selected for copy-number analysis by SNP array. WES was performed on six regions from PGL1, two from PGL3, one from PGL2 and PGL4 in addition to germline DNA, to identify somatic mutations and somatic copy-number alterations (SCNA) (**Supplementary Tables 1 and 2**). Targeted amplicon sequencing was used to validate a subset of somatic variants showing good concordance with WES (**Supplementary Table 3**).

This article is protected by copyright. All rights reserved.

All PGL tumours had low mutation frequencies (0.02-0.17 mutations per megabase) and low-level genomic instability as a percentage of genome altered (12.9-17.3%). Multi-region analysis of PGL1 and PGL3 revealed varying degrees of intra-tumoral heterogeneity. With regard to the smaller of the two tumours PGL3, the two regions analysed showed an identical SCNA profile (losses of chr1p, chr3 and chr11) and 6/17 overlapping somatic mutations (**Supplementary Figure 1**). A greater level of intra-tumoral heterogeneity was observed in PGL1, with only a single common mutation detected across tumour regions (**Figure 1C**). With respect to SCNAs in PGL1, loss of chr1p and chr18q12.2-23 were common and therefore early events (**Supplementary Figure 2**). Loss of chr18q11.2-12.2 and chr2q were present clonally in five (1.1.1, 1.1.3, 1.2.1, 1.2.2, 1.2.3) and three (1.1.1, 1.1.3, 1.2.1) of six regions sampled, respectively, and sub-clonally in two regions (1.2.4 and 1.2.2, respectively), suggesting they were later events. A Bayesian clustering method (PyClone) was used to identify clonal populations in PGL1 using the mutation data. In instances where the algorithm appeared overly aggressive in grouping mutations, the output was manually refined. Mutational clusters represented nine distinct cell populations (M^{A-I}), further highlighting the relative heterogeneity within tumour-PGL1.

A comparison between primary PGL tumours (PGL1-4) revealed no recurrently mutated genes, but some common SCNA events (**Figure 1D**). To interpret the frequency of these SCNAs in a larger series of PPGL tumours, we analysed SNP-array data from two published studies summarising the frequency of chromosome level changes[13,14]. As SCNAs in PPGL are dependent on gene driver and tumour gene-expression profile, we summarised the data with respect to four gene-expression subtypes (i.e. VHL, SDHx, RTK/C1A and MAX-

This article is protected by copyright. All rights reserved.

Author Manuscript

like/C2B) (**Supplementary Table 4**). As expected, PGL1-4 exhibited obligate loss of wild-type *SDHB* involving chr1p. Subclonal chr3 loss was also observed in PGL1, PGL2 and PGL3, although loss of chr3p and chr3q is relatively common in PPGL (all tumours: 28-51%, SDHx: 36%) and therefore these common events may be expected by chance. On the contrary, loss of chr2q involving the same chromosomal copy, an infrequent event in PPGL (All tumours: 5.5%, SDHx: 7%), was observed in tumours PGL1 and PGL4 (**Supplementary Figure 3**). The binomial probability of losing the same copy of chr2q in two of four synchronous *SDHB* PPGL tumours is low (0.013), providing circumstantial evidence of evolutionary convergence.

Bilateral *RET* and *MAX*-associated phaeochromocytoma

Intrigued by the observation of apparent convergent SCNAs in case C1, we interrogated three additional cases involving bilateral phaeochromocytoma (C2, C3 and C4). Germline *RET* mutations were present in cases C2 (NM_020975: c.1900T>C, NP_066124: p.Cys634Arg) and C3 (NM_020975: c.2753T>C p.Met918Thr).-A third case- (C4) had a germline *MAX* mutation (NM_002382: c.200C>A, NP_002373.3:p.Ala67Asp) and involved metachronous bilateral adrenal tumours that were removed 10 years apart. WES was applied to single regions sampled from left (PCC1) and right (PCC2) adrenal tumours in each case in addition to the respective matching germline DNA.

The mutation frequency was low in all tumours (0.09-0.18 mutations per Mb) and there were no commonly mutated genes. Tumours from case C2 displayed the highest level of genomic instability, having 25-29% of the genome altered. Tumours from cases C3 and C4 were

This article is protected by copyright. All rights reserved.

Author Manuscript

comparatively quiet, with 7.5-9.9% of the genome altered. Strikingly, a number of convergent SCNAs were detected between the matched primary *RET* tumours (**Figure 2**, **Supplementary Figures 4-6**). Case C2 had the largest number of convergent events involving common allelic loss of chr1p, chr3, chr8 and chr18p and alternate allelic loss of chr21. Primary tumours from case C3 had identical SNCA profiles, consisting of only two events involving ch1p and chr7q, with chr7p loss involving alternate chromosome copies. The metachronous tumours from case C4 had a more divergent SCNA profile and had only one convergent event involving loss of chr14q, being the expected second hit required for loss of wild type *MAX*. In summary, highly convergent SCNAs were detected in synchronous *RET* primary phaeochromocytomas, while a more divergent profile was observed in the metachronous *MAX* tumours.

Multi-tumour analysis of medullary thyroid carcinoma

We next analysed multifocal MTC arising in a thirty-year old female (C5) who also presented with synchronous bilateral phaeochromocytoma. PET/CT imaging with ^{18}F-FDG revealed minimally avid hypodense right (4cm) and left (1cm) adrenal masses, as well as mildly avid right lung metastasis, a central right liver metastasis, and osseous metastases involving the pelvis, bilateral scapulae, humerii, and femora (**Figure 3A**). A region of intense tracer uptake was seen in the right lobe of the thyroid and nearby cervical lymph nodes, which was confirmed to be MTC via histological analysis of a tumour biopsy. PET/CT with GaTate demonstrated intense avidity in both adrenal masses with limited avidity in the thyroid, nodal metastases, and distant metastases (**Figure 3A**). SPECT/CT with ^{123}I-MIBG mirrored the GaTate tracer pattern (**Figure 3A**). The patient underwent total thyroidectomy, resection of

This article is protected by copyright. All rights reserved.

Author Manuscript

the cervical lymph nodes, and right adrenalectomy. Diagnostic sequencing revealed a germline mutation in *RET* (NM_020975: NP_066124: c.1901G>A, p.Cys634Tyr) consistent with a diagnosis of MEN2A.

Fresh tissue specimens were obtained following surgical resection. These included a single tumour region from the right thyroid lobe ($T1^{Fresh}$) and a cervical lymph node metastasis ($T1^{Met}$)(**Figure 3B, 3C**). The remaining MTC tissue was fixed in formalin. FFPE specimens representing the right and left lobes of the thyroid gland were sectioned and stained with haemotoxylin and eosin and by immunohistochemistry for the cellular proliferation marker Ki-67. Review of Ki-67 staining of the right lobe of the thyroid revealed distinctive regions of high and low Ki-67 expression. As Ki67 expression has been shown to clinically correlate with metastatic disease[25], two regions representing high ($T1^{Ki67Hi}$) and low ($T2^{Ki67Lo}$) expression were needle-dissected for DNA extraction (**Figure 3D**). Closer analysis of sections from the left thyroid lobe revealed a small region of dysplastic growth also detected by FDG-PET (T3) (**Figure 3A and E**). The right adrenal PCC was sampled from two opposing poles and a genomic analysis of this tumour has been previously described[14]. Blood plasma cfDNA isolated from peripheral blood was taken prior to surgery. WES was performed on all fresh-frozen, FFPE, and cfDNA samples. High-resolution SCNA profiling was performed using the CytoScan HD or OncoScan FFPE assay on fresh frozen and FFPE samples, respectively.

Analysis of SCNA and somatic mutations in MTC primaries (T1-T3) showed no overlapping mutations and distinct SCNA profiles between primaries T1, $T2^{Ki67Lo}$ and T3 and the phaeochromocytoma, confirming that $T2^{Ki67Lo}$ was an independent primary despite co-location

This article is protected by copyright. All rights reserved.

Author Manuscript

with T1 (**Figure 4A**). In contrast, $T1^{Fresh}$, $T1^{Ki67Hi}$, and $T1^{Met}$ had significant overlap of SCNAs and somatic mutations (described below). Analysis of cfDNA detected 28 variants; 22 of these were ubiquitous amongst T1, $T1^{Ki67Hi}$, and $T1^{Met}$, two were shared between $T1^{Fresh}$ and $T1^{Met}$ but absent in $T1^{Ki67Hi}$, two were private to $T1^{Met}$, and two were found only in the cfDNA. No variants private to $T2^{Ki67Lo}$ and T3 could be detected in the cfDNA. We concluded that most DNA in blood plasma was released from one or more metastatic sites representing clone T1.

Although no recurrently mutated genes were observed between MTC T1-T3, we identified recurrent SCNAs. Notably, chr10 SCNAs were ubiquitous in MTC primaries, resulting in the enrichment of the mutant *RET* allele (RET^{MUT}) due to either somatic gain of RET^{MUT}, loss of wild type (RET^{WT}) or a combination of both events resulting in copy-neutral LOH (CNLOH) (**Supplementary Figure 7**). Allelic imbalances involving *RET* are known to be common in *RET*-driven phaeochromocytoma and MTC[26-28]. Primary tumours T1 and T3 also shared common loss events involving chr1p, chr4q, chr9 and chr22. A systematic comparison of SCNA frequencies found here in MTC to a larger series of MTC is hindered by the availability of such datasets.

Multi-region analysis involving $T1^{Fresh}$, $T1^{Ki67Hi}$, and $T1^{Met}$ enabled mapping of clonal evolution (**Figure 4B, 4C**). Almost half of the mutations (22/47) were shared between the T1 samples. Truncal events with the highest VAF included missense mutations in *FCAMR* and *MAX*. With respect to the tumour suppressor gene *MAX*, three mutation effect algorithms (SIFT, PolyPhen, Condel) classified the mutation to be damaging. Furthermore, loss of wild type *MAX* supported a tumour suppressor function. Mutation clustering and manual interpretation

This article is protected by copyright. All rights reserved.

Author Manuscript

of SCNA data was used to build an evolutionary map of primary T1 (**Figure 4C**). Chromosomes 3, 9, and 22 were lost at a similar frequency to chr1p in $T1^{Ki67Hi}$ and $T1^{Met}$. Loss of chr3 and chr9 was present in only a reduced proportion of cells in $T1^{Fresh}$ with no loss of chr22 evident. Analysis of B-allele frequency demonstrated that $T1^{Ki67Hi}$ and $T1^{Met}$ had lost opposite copies of both chr3 and chr22, indicating independent and late events. While this may also be the case for chr9, allele enrichment demonstrated loss of the same copy in both clones; therefore it is not possible to determine the timing of this event. Interestingly, different chr10 alterations (involving *RET*) were observed between T1 tumour regions (**Supplementary Figure 7**). Our interpretation of the data is that duplication of RET^{Mut} most likely occurred as an early event. Loss of RET^{WT} occurred later in $T1^{Ki67Hi}$ and a majority of cells in $T1^{Fresh}$ either as a common ancestral event or as two independent events in different subclones, depending on interpretation of the chr9 loss, as previously discussed. Regardless of the timing, there appears to be a further selective advantage to losing RET^{WT}, consistent with our observation of RET^{WT} loss without RET^{Mut} duplication in primary $T2^{Ki67Lo}$. Independent alterations of chromosomes 3, 9, 10 and 22 illustrate clear examples of convergent evolution during MTC development.

Discussion

We have performed a detailed genomic analysis of synchronous and metachronous hereditary endocrine tumours. Consistent with prior studies, PPGL and MTC have relatively quiet genomes: they have a low mutation frequency and exhibit few but recurrent chromosome-level changes[13,14]. Varying degrees of tumour heterogeneity were observed within primary PGL, with ongoing acquisition of tertiary mutations and SCNAs. We have

This article is protected by copyright. All rights reserved.

Author Manuscript

demonstrated clonal evolution within hereditary MTC using multi-region analysis of tumour tissue and circulating cfDNA. Metastatic MTC exhibited branched-chain evolution and several convergent events involving SCNAs. Our most striking observation, however, was the apparent parallel evolution between synchronous primary PPGL, which may suggest shared genetic contingencies that dictate tumour evolution and convergence.

Genomic studies of PPGL have begun to catalogue the recurrent somatic changes that co-operatively drive tumorigenesis. For instance, WES has identified mutations in genes associated with chromatin modification, telomere maintenance, DNA damage response and kinase signalling[13,14,29]. However, few genes (outside of known PPGL drivers) are recurrently mutated. We have shown that only a fraction of somatic mutations can be shared ancestral events in familial PPGL. In the largest PGL tumour analysed (PGL1), only a single truncal mutation was found, in the vitamin B_{12} carrier-protein *TCN2*. Although vitamin B_{12} is a cofactor for several important enzymatic reactions, the TCN2 protein activity is largely cell-extrinsic, where it facilitates the delivery and importation of vitamin B12 into the cell, after which the protein undergoes lysosomal degradation[30]. The pathogenicity of the *TCN2* mutation cannot be confirmed without functional validation. However, since *TCN2* mutations have not been previously observed in PPGL a more parsimonious explanation is that such mutations are passenger rather than driver events. Regardless, small-scale (point) mutations appear not to be be important for early PPGL tumorigenesis as judged by the present analysis.

In contrast to small-scale mutations, large chromosomal imbalances are recurrent in PPGL and frequently reflect the underlying driver mutation[13]. Our data provides evidence that

This article is protected by copyright. All rights reserved.

Author Manuscript

infrequent chromosomal changes, such as loss of chr2q, are also co-operative and may confer growth advantage through being late and convergent events between paired primaries. Identifying putative tumour suppressor genes within chr2q is difficult, given the chromosome arm-level imbalance, which is typical for PPGL. Loss of the same copy of 2q in two independent primary tumours may suggest an occult pathogenic mutation on chr2q; however, we could not identify a plausible gene candidate from the germline WES data (**Supplementary Table 5**). Alternatively, it is possible that allele-specific loss of heterozygosity is due to other mechanisms, including silencing of the retained allele by DNA methylation or haploinsufficiency of one or many genes[31].

MTC represents a prototypical oncogene-driven cancer, involving either constitutional or somatic *RET* mutations driving neoplastic transformation of parafollicular cells. With the exception of somatic *RAS* mutations, few other genes are recurrently mutated in MTC[32,33]. Here we have identified *MAX* as a putative tumour suppressor gene in MTC. The tumour suppressor function of *MAX* in PPGL is already well known [34,35], but there is mounting evidence for a more general role for *MAX* in neuroendocrine tumour biology. A recent study in small cell lung cancer (SCLC) encompassing 53 cell lines and 45 primary tumours found MAX-inactivating alterations in 6% of SCLCs tested[36]. Restoring wild type MAX expression in either *MAX*-mutant SCLC or phaeochromocytoma was found to induce neuroendocrine differentiation and reduce cellular proliferation[36,37]. We propose that MAX may have similar tumour suppressor function in parafollicular cells. Analysis of a large tumour series will be required to determine the frequency of *MAX* mutations in MTC.

Author Manuscript

This article is protected by copyright. All rights reserved.

Like PPGL, MTC harbours few but recurrent regions of copy-number change. We observed considerable diversity between synchronous MTC primary tumours, with the highest degree of genome instability and mutation load associated with the metastatic phenotype. Progression from primary to metastatic disease in clone T1 was associated with additional somatic events; however, significant heterogeneity was also observed across different sampled regions of the primary tumour, indicating sustained genomic instability. Importantly, despite the marked heterogeneity observed between tumour clones, all tumours involved selective enrichment of mutant *RET* through chromosomal duplication, loss of the wild type copy or a combination of both events. Our data confirms that the dominant effect of mutant *RET* is likely to confer a strong selective advantage to MTC tumour cells and that increases in gene dosage occur during tumour evolution.

Few studies have performed genomic profiling of multi-focal primary tumours. Two prior studies involving hereditary renal cell carcinoma (RCC) concluded that synchronous or metachronous VHL-associated tumours are as genetically different from each other as they are from other unrelated individuals[8,38]. Fisher and colleagues proposed that the divergent genetic profiles found in RCC are likely contingent on early somatic events, but convergence on the PI3K-AKT-mTOR signaling pathway was still a common feature[8]. It is interesting that we have observed stronger evidence for parallel evolution in synchronous PPGL, not only by the detection of common SCNAs, but also the similarity in the degree of genome instability between the matched PPGL tumours when compared to other cases. We propose that the convergent evolutionary trajectory of the synchronous PPGL may be contingent upon pre-existing disease-modifying variants in the germline, or alternatively, early somatic changes (genetic or epigenetic) in neural crest progenitor during embryogenesis. The latter

This article is protected by copyright. All rights reserved.

Author Manuscript

would be in keeping with a unifying theory of PPGL tumorigenesis that links disparate PPGL driver genes and pathways to a common failure of neuronal apoptosis during early embryonic development[39]. However, in the absence of common ancestral genetic changes that link back to a common cell of origin, this is difficult to prove. A more comprehensive analysis involving whole-genome sequencing may reveal shared events in non-coding regions, somatic rearrangements and small focal SCNA changes undetected by WES. Support for the notion that early somatic events, rather than constitutional germline variants, steer tumour progression comes from our observation that metachronous tumours, as in case C4, have a more diverse genetic profile. However, this single case involves a different genetic driver to the other synchronous PPGL used in our study, so analysis of additional cases is required.

Questions remain regarding why some endocrine tumours metastasise while others take a more indolent course. It also remains unclear whether metastatic potential is stochastic and programmed early in tumorigenesis, or alternatively develops with time. Answering these questions through a systematic analysis of benign and malignant tumours is confounded by the higher metastatic risk associated with specific driver genes or genotypes, raising the possibility that different pathways and mechanisms may lead to metastasis in different tumour groups. Individual disease subtypes or genotypes therefore need to be analysed in isolation to avoid such confounding issues. One recurring feature reported in endocrine neoplasia is the higher degree of genetic instability and tumour heterogeneity in many (albeit not all) metastatic tumours[12,40,41]. Early genome changes during tumorigenesis that create a genetically unstable phenotype may set the stage by increasing the chances of acquiring additional genetic changes that enable the cell to invade adjacent tissues and colonise distant sites.

This article is protected by copyright. All rights reserved.

Author Manuscript

The analysis of tumours from hereditary endocrine syndromes is a powerful approach to understand clonal evolution and we have observed convergent evolution both between and within tumour clones. The analysis of a larger series involving synchronous primary tumours that display discordant metastatic potential may be useful for identifying changes required for metastasis in these tumour types.

Author Contributions

AF, RCB, BR, RHJ and RWT conceived the study. AF and TD performed experiments and analysis. SD, AJC, SF and AG performed pathology review and analysis. HT, CD, CY, ELD, JH and JAM provided material support. DB, ELD, AT, AH and PJ recruited patients and curated clinical data. JL performed data analysis. AF and RWT wrote the manuscript. All authors have seen and approved the final manuscript.

Acknowledgements

This project was supported by the Australian National Health and Medical Research Council and Hillcrest Foundation (Perpetual Trustees). We thank Joshy George and Ismael Vergara for advice on genomic analysis, staff of the Peter Mac Molecular Genomics Facility and the Victorian Cancer Biobank and all patients included in the study for their contribution.

References

1. Zhang Y, Nose V. Endocrine tumors as part of inherited tumor syndromes. *Adv Anat Pathol* 2011; **18**: 206-218.

This article is protected by copyright. All rights reserved.

Author Manuscript

2. Dahia PL. Pheochromocytoma and paraganglioma pathogenesis: learning from genetic heterogeneity. *Nat Rev Cancer* 2014; **14**: 108-119.

3. Kim TM, Jung SH, An CH*, et al.* Subclonal genomic architectures of primary and metastatic colorectal cancer based on intratumoral genetic heterogeneity. *Clin Cancer Res* 2015; **21**:4461-72.

4. Boutros PC, Fraser M, Harding NJ*, et al.* Spatial genomic heterogeneity within localized, multifocal prostate cancer. *Nat Genet* 2015; **47**: 736–745.

5. Kim TM, Jung SH, Baek IP*, et al.* Regional biases in mutation screening due to intratumoural heterogeneity of prostate cancer. *J Pathol* 2014; **233**: 425-435.

6. Zhang J, Fujimoto J, Zhang J*, et al.* Intratumor heterogeneity in localized lung adenocarcinomas delineated by multiregion sequencing. *Science* 2014; **346**: 256-259.

7. Jamal-Hanjani M, Hackshaw A, Ngai Y*, et al.* Tracking genomic cancer evolution for precision medicine: the lung TRACERx study. *PLoS biology* 2014; **12**: e1001906.

8. Fisher R, Horswell S, Rowan A*, et al.* Development of synchronous VHL syndrome tumors reveals contingencies and constraints to tumor evolution. *Genome Biol* 2014; **15**: 433.

9. Bashashati A, Ha G, Tone A*, et al.* Distinct evolutionary trajectories of primary high-grade serous ovarian cancers revealed through spatial mutational profiling. *J Pathol* 2013; **231**: 21-34.

10. Kim H, Zheng S, Amini SS*, et al.* Whole-genome and multisector exome sequencing of primary and post-treatment glioblastoma reveals patterns of tumor evolution. *Genome Res* 2015.

This article is protected by copyright. All rights reserved.

Author Manuscript

11. Gerlinger M, Rowan AJ, Horswell S*, et al.* Intratumor heterogeneity and branched evolution revealed by multiregion sequencing. *N Engl J Med* 2012; **366**: 883-892.

12. Crona J, Backman S, Maharjan R*, et al.* Spatio-temporal heterogeneity characterizes the genetic landscape of pheochromocytoma and defines early events in tumourigenesis. *Clin Cancer Res* 2015; **21**:4451-60

13. Castro-Vega LJ, Letouze E, Burnichon N*, et al.* Multi-omics analysis defines core genomic alterations in pheochromocytomas and paragangliomas. *Nat Commun* 2015; **6**: 6044.

14. Flynn A, Benn D, Clifton-Bligh R*, et al.* The genomic landscape of phaeochromocytoma. *J Pathol* 2015; **236**: 78-89.

15. Li H, Durbin R. Fast and accurate short read alignment with Burrows-Wheeler transform. *Bioinformatics* 2009; **25**: 1754-1760.

16. Cibulskis K, Lawrence MS, Carter SL*, et al.* Sensitive detection of somatic point mutations in impure and heterogeneous cancer samples. *Nat Biotechnol* 2013; 31(3):213-9

17. Roth A, Ding J, Morin R*, et al.* JointSNVMix: a probabilistic model for accurate detection of somatic mutations in normal/tumour paired next-generation sequencing data. *Bioinformatics* 2012; **28**: 907-913.

18. Larson DE, Harris CC, Chen K*, et al.* SomaticSniper: identification of somatic point mutations in whole genome sequencing data. *Bioinformatics* 2012; **28**: 311-317.

19. Koboldt DC, Chen K, Wylie T*, et al.* VarScan: variant detection in massively parallel sequencing of individual and pooled samples. *Bioinformatics* 2009; **25**: 2283-2285.

This article is protected by copyright. All rights reserved.

Author Manuscript

20. McKenna A, Hanna M, Banks E*, et al.* The Genome Analysis Toolkit: a MapReduce framework for analyzing next-generation DNA sequencing data. *Genome Res* 2010; **20**: 1297-1303.

21. Lefebure M, Tothill RW, Kruse E*, et al.* Genomic characterisation of Eμ-Myc mouse lymphomas identifies Bcor as a Myc co-operative tumour-suppressor gene *Nature Communications* 2017; **Accepted**.

22. Favero F, Joshi T, Marquard AM*, et al.* Sequenza: allele-specific copy number and mutation profiles from tumor sequencing data. *Ann Oncol* 2015; **26**: 64-70.

23. Roth A, Khattra J, Yap D*, et al.* PyClone: statistical inference of clonal population structure in cancer. *Nature methods* 2014; **11**: 396-398.

24. Flynn A, Dwight T, Harris J*, et al.* Pheo-Type: A Diagnostic Gene-expression Assay for the Classification of Pheochromocytoma and Paraganglioma. *J Clin Endocrinol Metab* 2016; **101**: 1034-1043.

25. Li LT, Jiang G, Chen Q*, et al.* Ki67 is a promising molecular target in the diagnosis of cancer (review). *Mol Med Rep* 2015; **11**: 1566-1572.

26. Huang SC, Koch CA, Vortmeyer AO*, et al.* Duplication of the mutant RET allele in trisomy 10 or loss of the wild-type allele in multiple endocrine neoplasia type 2-associated pheochromocytomas. *Cancer Res* 2000; **60**: 6223-6226.

27. Koch CA, Huang SC, Moley JF*, et al.* Allelic imbalance of the mutant and wild-type RET allele in MEN 2A-associated medullary thyroid carcinoma. *Oncogene* 2001; **20**: 7809-7811.

Author Manuscript

This article is protected by copyright. All rights reserved.

28. Ciampi R, Romei C, Cosci B*, et al.* Chromosome 10 and RET gene copy number alterations in hereditary and sporadic Medullary Thyroid Carcinoma. *Mol Cell Endocrinol* 2012; **348**: 176-182.

29. Toledo RA, Qin Y, Cheng ZM*, et al.* Recurrent Mutations of Chromatin-Remodeling Genes and Kinase Receptors in Pheochromocytomas and Paragangliomas. *Clin Cancer Res* 2016; **22**: 2301-2310.

30. Gherasim C, Lofgren M, Banerjee R. Navigating the B(12) road: assimilation, delivery, and disorders of cobalamin. *J Biol Chem* 2013; **288**: 13186-13193.

31. Ryland GL, Doyle MA, Goode D*, et al.* Loss of heterozygosity: what is it good for? *BMC Med Genomics* 2015; **8**: 45.

32. Agrawal N, Jiao Y, Sausen M*, et al.* Exomic sequencing of medullary thyroid cancer reveals dominant and mutually exclusive oncogenic mutations in RET and RAS. *J Clin Endocrinol Metab* 2013; **98**: E364-369.

33. Cai J, Li L, Ye L*, et al.* Exome sequencing reveals mutant genes with low penetrance involved in MEN2A-associated tumorigenesis. *Endocr Relat Cancer* 2015; **22**: 23-33.

34. Burnichon N, Cascon A, Schiavi F*, et al.* MAX Mutations Cause Hereditary and Sporadic Pheochromocytoma and Paraganglioma. *Clin Cancer Res* 2012; **18**: 2828-2837.

35. Comino-Mendez I, Gracia-Aznarez FJ, Schiavi F*, et al.* Exome sequencing identifies MAX mutations as a cause of hereditary pheochromocytoma. *Nat Genet* 2011; **43**: 663-667.

Author Manuscript

This article is protected by copyright. All rights reserved.

36. Romero OA, Torres-Diz M, Pros E*, et al.* MAX inactivation in small cell lung cancer disrupts MYC-SWI/SNF programs and is synthetic lethal with BRG1. *Cancer Discov* 2014; **4**: 292-303.

37. Qin N, de Cubas AA, Garcia-Martin R*, et al.* Opposing effects of HIF1alpha and HIF2alpha on chromaffin cell phenotypic features and tumor cell proliferation: Insights from MYC-associated factor X. *Int J Cancer* 2014; **135**: 2054-2064.

38. Beroukhim R, Brunet JP, Di Napoli A*, et al.* Patterns of gene expression and copy-number alterations in von-hippel lindau disease-associated and sporadic clear cell carcinoma of the kidney. *Cancer Res* 2009; **69**: 4674-4681.

39. Lee S, Nakamura E, Yang H*, et al.* Neuronal apoptosis linked to EglN3 prolyl hydroxylase and familial pheochromocytoma genes: developmental culling and cancer. *Cancer Cell* 2005; **8**: 155-167.

40. Sandgren J, Diaz de Stahl T, Andersson R*, et al.* Recurrent genomic alterations in benign and malignant pheochromocytomas and paragangliomas revealed by whole-genome array comparative genomic hybridization analysis. *Endocr Relat Cancer* 2010; **17**: 561-579.

41. Flicker K, Ulz P, Hoger H*, et al.* High-resolution analysis of alterations in medullary thyroid carcinoma genomes. *Int J Cancer* 2012; **131**: E66-73.

Author Manuscript

This article is protected by copyright. All rights reserved.

Author Manuscript

Table 1. **Patients and samples analysed**

Study ID	Age at Diagnosis (years)	Age at Surgery (years)	Gender	Gene	Germline mutation AA/CDS change	Diagnosis	Pathology	Tumours	Regions Analysed
C1	23	23	M	SDHB	NP_002991: p.Gln30ArgfsTer47 NM_003000: c.88delG	PGL2 Multifocal PGL	Benign	PGL1	Exome (4) CytoScan (1)
								PGL2	Exome (1) CytoScan (1)
								PGL3	Exome (2) CytoScan (1)
								PGL4	Exome (1) CytoScan (1)
C2	21	21	F	RET	NP_066124: p.Cys634Arg NM_020975: c.1900T>C	MEN2A bilateral PC bilateral MTC PGL (thoracic)	BenignPC/ Metastatic MTC	PCC1	Exome(1)
								PCC2	Exome(1)
C3	25	25	F	RET	NP_066124: p.Met918Thr NM_020975: c.2753T>C	MEN2B Bilateral PC	Benign	PCC1	Exome(1)
								PCC2	Exome(1)
C4	23	23,33	F	MAX	NP_002373.3: p.Ala67Asp NM_002382: c.200C>A	Right PC at 23 Left-PC at 33	Benign	PCC1	Exome(1)
								PCC2	Exome(1)
C5	30	30	F	RET	NP_066124: p.Cys634Tyr NM_020975: c.1901G>A	MEN2A Bilateral PC Bilateral MTC	Benign PC/ Metastatic MTC	T1 (+HiKi67)	Exome(2) CytoScan (1) Oncoscan (1)
								T1-Met	Exome(1) CytoScan (1)

This article is protected by copyright. All rights reserved.

		T2	Exome(1) OncoScan (1)
		T3	Exome(1) OncoScan (1)

(AA, amino acid; CDS, coding DNA sequence; PGL, paraganglioma; PC, phaeochromocytoma, MTC, medullary thyroid carcinoma)

Author Manuscript

This article is protected by copyright. All rights reserved.

Figure Legends

Figure 1. Intra- and inter-tumoral analysis of synchronous SDHB-associated paraganglioma from case C1

(A) 68Ga-DOTA-octreotate (GaTate) and 18F-FDG PET imaging of four synchronous paragangliomas used for genomic analysis (B) Schematic representation of multi-region sampling from paraganglioma (C) Clonal evolution analysis of primary PGL1, including: i) The clonal evolution map inferred from SCNA and mutation cluster analysis for PGL1. ii) B-allele frequency of chr2q, showing divergence from 50% indicating loss of heterozygosity in four of six regions sampled. iii) Shared and private variants detected in regions sampled, including cluster classification based on PyClone (P) and manual classification (M). (D) High-resolution SNP array analysis of four synchronous primary paragangliomas.

Figure 2. SCNA profiles from synchronous PPGL

Comparative analysis of SCNA profiles from synchronous PPGL tumours. Also included are the population frequencies of the respective chromosome arm-level changes observed in a large series of PPGL tumours; the data has been stratified by tumour genotype or gene-expression subtype.

Figure 3. Clinical presentation and tumour sampling from MEN2 case C5.

Author Manuscript

This article is protected by copyright. All rights reserved.

(A) Molecular imaging of MTC and PCC. 18F-FDG PET showing minimal tracer uptake in right and left adrenal masses, and moderate uptake in right lung, central right liver, and osseous metastases. A region of intense tracer uptake can be seen in the right lobe of the thyroid and nearby cervical lymph nodes. GaTate PET/CT and 123I-MIBG SPECT/CT both demonstrated intense avidity in the adrenal masses with minimal to no avidity in the thyroid, nodal metastases, and distal metastases. Red arrow indicates level of adrenal glands. (B) Thyroid gland following surgical resection. The sliver of tissue marked by a white outline was taken from the right thyroid and snap-frozen for genomic profiling (specimen T1Fresh). (C) FFPE section of cervical node stained with haematoxylin and eosin. Specimen T1Met was obtained as fresh frozen tissue from a proximal node. (D) FFPE section of right thyroid tumour stained against Ki-67. The regions of high Ki-67 (specimen T1Ki67Hi), and low Ki-67 (specimen T2Ki67Lo) used for genomic profiling are marked with black outlines. (E) FFPE section of left thyroid stained against Ki-67. The region extracted for genomic profiling is marked by a black outline (specimen T3).

Figure 4. Genomic analysis of tumours taken from MEN2 case C5.

(A) Summary of comparative SCNA profiles from MTC and PCC tumour samples (F = T1Fresh, Ki67 = T1Ki67Hi, T2 = T2Ki67Lo, M = T1Met). (B) Heatmap showing VAFs for somatic mutations (rows) detected in any MTC specimen (columns). Values in the PyClone and Manual columns indicate the cluster each mutation was assigned by the respective method. Mutation consequence is denoted as synonymous (black text) or nonsynonymous (red text). (C) Schematic depicting the evolution of various subclones (horizontal axis)

This article is protected by copyright. All rights reserved.

Author Manuscript

through the sequential accrual of genomic alterations over time (vertical axis). Copy-number alterations are denoted as chromosome number, arm, and event type (- and +, respectively loss and gain). Clusters of mutation events are denoted with the letter M with a superscript annotation of the cluster, as determined by PyClone with manual adjustment. Values in brackets indicate which chromosomal copy was lost, as mutant (m), wild-type (wt), and allele set A/B. Shaded lines and text indicate an alternative evolutionary path based on common or shared changes that cannot be resolved.

Author Manuscript

This article is protected by copyright. All rights reserved.

Supplementary Data

Supplementary Figure 1: Somatic copy number analysis of PGL3 of case C1

Supplementary Figure 2: Somatic copy number analysis of PGL1 of case C1

Supplementary Figure 3: chr2q loss in PGL1 and PGL4 of case C1

Supplementary Figure 4: Somatic copy number analysis of case C2

Supplementary Figure 5: Somatic copy number analysis of case C3

Supplementary Figure 6: Somatic copy number analysis of case C4

Supplementary Figure 7: Chromosome 10 somatic copy number alterations in MTC from C5

Supplementary Table 1: WES high confidence somatic mutations

Supplementary Table 2: Percentages of genome affected by somatic copy number alterations

Supplementary Table 3: Deep sequencing for validation of variants detected by exome sequencing

Supplementary Table 4: Frequency of autosomal somatic copy number alterations within PPGL subtypes

Supplementary Table 5: Predicted deleterious germline variants enriched by loss of chromosome 2q in PGL1 and PGL4 of case C1

Author Manuscript

This article is protected by copyright. All rights reserved.

Author Manuscript

This article is protected by copyright. All rights reserved.

Author Manuscript

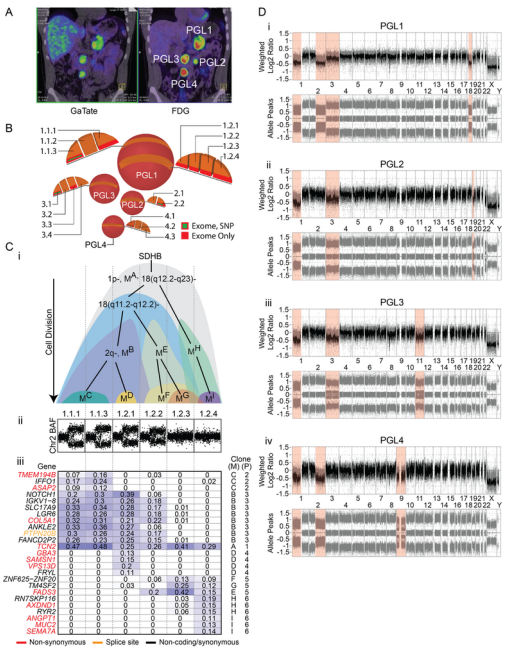

PATH_4900_Fig1.tif

This article is protected by copyright. All rights reserved.

Author Manuscript

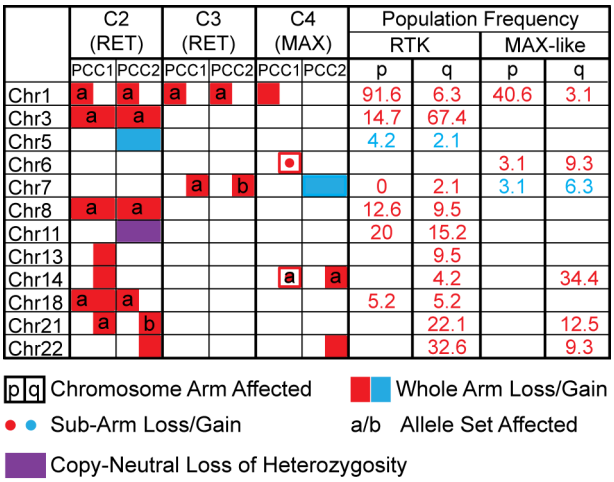

PATH_4900_Fig2.tif

This article is protected by copyright. All rights reserved.

Author Manuscript

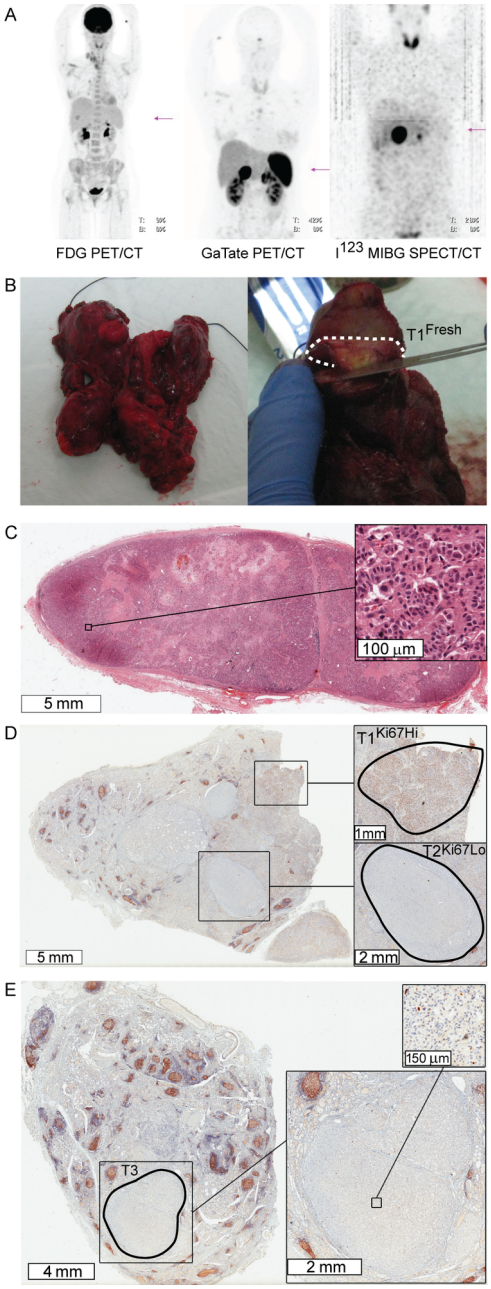

PATH_4900_Fig3.tif

This article is protected by copyright. All rights reserved.

Author Manuscript

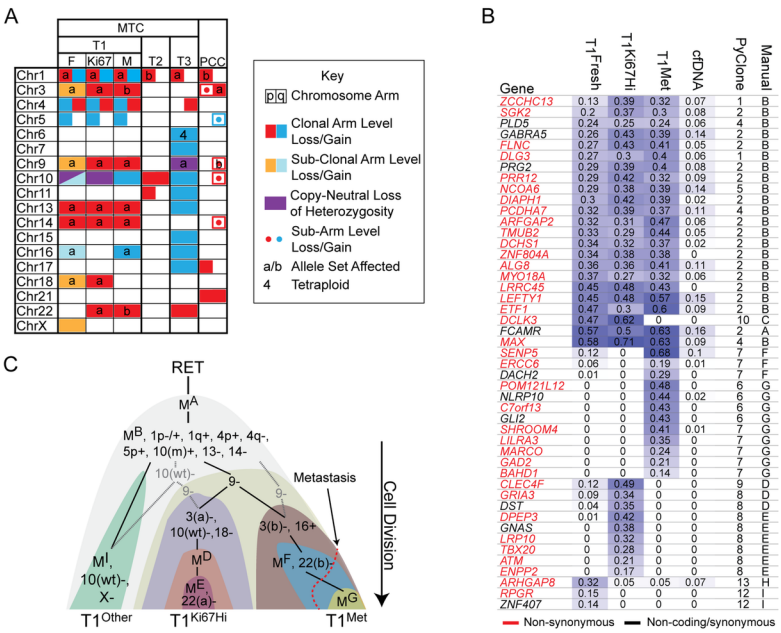

PATH_4900_Fig4.tif

This article is protected by copyright. All rights reserved.